American Mineralogist, Volume 78, pages 271–284, 1993

Brucite [$Mg(OH)_2$] dehydration and the molar volume of H_2O to 15 GPa

MARIE C. JOHNSON, DAVID WALKER
Lamont-Doherty Earth Observatory and Department of Geological Sciences, Columbia University, Palisades, New York 10964, U.S.A.

ABSTRACT

The dehydration of brucite to produce periclase and H_2O [$Mg(OH)_2 \leftrightarrow MgO + H_2O$] was experimentally investigated from 1 to 15 GPa in order to study the compressibility of H_2O at very high pressures. Low-pressure experiments were performed in a piston-cylinder apparatus and high-pressure experiments in a multianvil. The dehydration boundary was identified using both differential thermal analysis and quenching experiments. Thermal gradients present in the multianvil assemblies promoted thermal diffusion and allowed thermally compacted periclase to quench as periclase in quenching experiments performed at conditions outside the brucite stability field. Many experimental difficulties were encountered, including obtaining pure brucite starting material, preventing contamination by the pressure medium, and assuring that H_2O leakage did not occur during the experiment. This dehydration equilibrium is especially vulnerable to these types of problems, and special care was required to reduce these sources of error. The resulting experimental data indicate that the reaction boundary has a positive dP/dT slope to 15 GPa and is nearly vertical above 6 GPa (~1200 °C). These new data are combined with thermodynamic and *PVT* properties of brucite and periclase in order to calculate the molar volume of H_2O along the dehydration curve. These calculations suggest that the molar volume of H_2O decreases from 21 cm^3 at 1 GPa and 845 °C to 10 cm^3 at 15 GPa and 1280 °C. These volumes are very similar to the molar volumes predicted using empirical modified Redlich-Kwong *PVT* models.

INTRODUCTION

Accurate thermodynamic data must be combined with reliable physical property data to understand and predict the behavior of materials at high pressures and temperatures in the Earth's mantle. The development of very high-pressure experimental techniques (multianvil, diamond-anvil) allows these kinds of data to be obtained under static conditions and bridges the gap between data collected using standard piston-cylinder techniques and data generated under the transient but super high-pressure conditions of shock waves. Most recent experimental data collected using these very high-pressure techniques concern the physical properties and phase equilibria of the principal anhydrous minerals found in the Earth's mantle. The physical properties (thermal expansion, bulk modulus) of hydrous minerals are largely unknown. The behavior of fluids (H_2O, CO_2, etc.) at very high pressures has not been widely investigated experimentally either, although a few shock wave studies exist (e.g., Rice and Walsh, 1957).

Knowledge of the pressure-volume-temperature relationship, or equation of state, of H_2O is crucially important because H_2O controls many physical properties, including melting temperature, extent of melting, viscosity, phase stability, and mineral relations. In addition, deep-focus earthquakes have been attributed to hydrous mineral dehydration in downgoing slabs (Meade and Jeanloz, 1991). A *PVT* relationship for H_2O would allow phase equilibria constraints on the stabilities and compositions of mantle hydrous phases to be calculated. Although several models of the *PVT* properties of H_2O at high pressure exist (e.g., Halbach and Chatterjee, 1982; Belonoshko and Saxena, 1991), these models could be further constrained by new experimental data at high pressures.

At pressures below 1 GPa, formidable experimental difficulties have been overcome, and the volume of H_2O has been measured directly as a function of pressure and temperature (Burnham et al., 1969). Although conceptually simple, this method has not been successfully applied at pressures greater than 1 GPa. At these high pressures, one of three approaches may be adopted. First, a theoretical *PVT* relationship can be derived using molecular dynamics (Belonoshko and Saxena, 1991; Brodholt and Wood, 1990). Second, an empirical *PVT* relationship can be deduced on the basis of a modified Redlich-Kwong (MRK) model (e.g., Kerrick and Jacobs, 1981; Holloway, 1981; Halbach and Chatterjee, 1982). Because these MRK models are purely empirical, they generally fit the data on which they are based extremely well but cannot be extrapolated with confidence to pressures and temperatures beyond this range. A few of these MRK models incorporate existing shock wave data for H_2O (Lyzenga

0003–004X/93/0304–0271$02.00

et al., 1982; Rice and Walsh, 1957) in order to calculate volumes at very high pressure. These shock wave data are limited, however, because temperature cannot be measured independently of pressure; it must be calculated using Hugoniot expressions.

A third option based on phase equilibria is adopted here. The slope of a univariant curve in pressure-temperature space is a function of the differences in volumes and entropies of the products and the reactants. For a simple dehydration equilibrium ($H \leftrightarrow A + nH_2O$), the slope of the curve depends on the thermodynamic and physical properties of H_2O, as well as the solid phases. If the volumes and entropies of the solid phases, H and A, and the entropy of H_2O are well known as functions of pressure and temperature, then the *PVT* relationship of the fluid can be calculated from the location of the equilibrium boundary.

Several restrictions must be met for this phase equilibria approach to yield useful data. For example, the heat capacities and bulk moduli of the solid phases must be well-known functions of temperature and pressure. The hydrous phase must break down by dehydration rather than by melting over a wide *P-T* range. Finally, the solid phases must not undergo pressure-induced polymorphic phase transitions, which cause discontinuities in the *P-T* slope. An ideal reaction that meets all three requirements is the dehydration of brucite to form periclase and H_2O [$Mg(OH)_2 \leftrightarrow MgO + H_2O$]. In addition, this reaction deserves special interest because the dehydration curve has been predicted to change from a positive to a negative slope at about 8 GPa (S. Saxena, personal communication). This predicted change in slope reflects the high compressibility of the fluid phase relative to the solid phases.

The brucite dehydration reaction has been the subject of much experimental effort at low pressures (<3 GPa) (i.e., Roy and Roy, 1957; Ball and Taylor, 1961; Barnes and Ernst, 1963; Weber and Roy, 1965; Yamaoka et al., 1970; Irving et al., 1977; Schramke et al., 1982). Many of these experimental studies produced contradictory results. For example, Yamaoka et al. (1970) reported that the slope of the dehydration curve changes from positive to negative at 3.2 GPa and 1000 °C. In a later investigation, these results were disproved, and a positive slope was recorded to 3.3 GPa (Irving et al., 1977). The discrepancy in results among different investigations may be largely attributed to difficulties in quenching this reaction; the kinetics of dehydration and rehydration are so rapid that periclase and H_2O tend to reform to brucite upon quench from high temperature and pressure. This tendency causes the brucite stability field to be overestimated. Furthermore, this reaction is vulnerable to the experimental environmental controls. Any cryptic leaks that allow H_2O to escape give $P_{H_2O} < P_{tot}$, and an artificially enhanced periclase stability field.

This difficulty with quenching is well recognized, and several in situ techniques have been developed to avoid quenching problems. For example, at pressures below 0.8 GPa, the volume of the sample was measured directly at pressure and temperature using a specially fitted internally heated pressure vessel (Schramke et al., 1982). Recent attempts to determine this reaction boundary at high pressures have used either in situ X-rays (Leinenweber et al., 1991) or differential thermal analysis [DTA] (Kanzaki, 1990, 1991).

This paper reports an experimental effort to determine accurately the brucite dehydration equilibrium from 1 to 15 GPa. The approach adopted here is a combination of DTA and quenching experiments. The quenching experiments are more reliably interpreted than in previous studies because thermal gradients cause diffusive migration of periclase and H_2O to different regions of the experimental charge. This separation facilitates quenching of periclase in experiments outside the brucite stability field. These new data are then used to calculate the volume of H_2O at pressures and temperatures along the reaction boundary. These calculated volumes are compared with volumes calculated using MRK *PVT* models.

Experimental techniques

Reconnaissance experiments were done using reagent-grade brucite obtained from Johnson Matthey. This brucite was found to contain 3 wt% impurities (mostly $CaCO_3$). Impurities will alter the brucite dehydration temperature. To avoid introducing this uncertainty, pure brucite had to be obtained. Therefore, brucite was synthesized hydrothermally from starting materials consisting of ultra-high purity 99.8% MgO (Ozark Tech.) and deionized, distilled H_2O. These starting materials were weighed, loaded into a Teflon vessel, placed in a large-capacity oven, and held at 225 °C for 48 h. The synthesis was terminated by shutting off power to the oven and letting the Teflon vessel cool down gradually. After cooling, the solid product was weighed; the weight gain indicated a 98.8% yield. Standard X-ray diffraction analysis revealed that the product was brucite, and no other phases were present. This new, pure starting material was used for all the quenching experiments reported here.

Experiments were performed from 1 to 15 GPa in two apparati using two techniques. The low-pressure experiments (≤4 GPa) were performed in standard piston cylinders of the type designed by Boyd and England using ½-in. furnace assemblies. All these experiments employed in situ DTA to detect the reaction boundary. Approximately 40 mg of brucite was loaded into a Pt capsule welded on both ends. MgO was used as filler rods, and S-type (100% Pt-Pt/10% Rh) thermocouples were used to monitor temperature. In order to produce a differential signal, two thermocouples were introduced into the sample region using a double junction thermocouple. The hot thermocouple was embedded directly in contact with the Pt capsule, while the cold thermocouple junction was ~5 mm above this junction. Graphite tubes served as heaters, and the pressure medium was $BaCO_3$.

The high-pressure experiments were performed in a multianvil device using a 600-ton press. The pressure

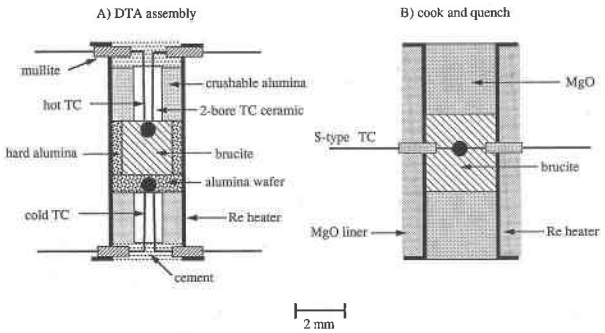

Fig. 1. Schematic diagram showing the two multianvil experimental assemblies. Scale bar is 2 mm in both cases. (**A**) Assembly for DTA experiments. (**B**) Assembly for quenching experiments.

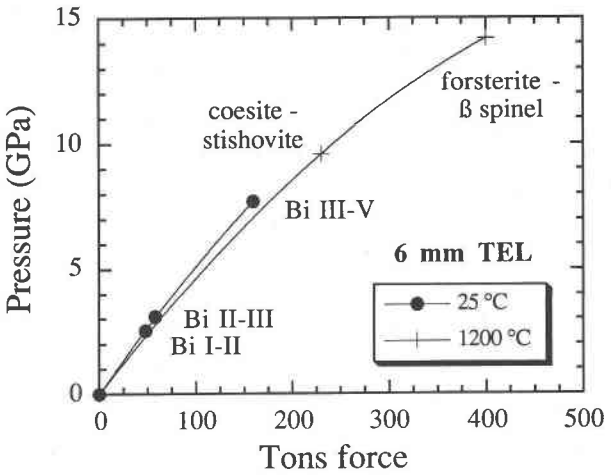

Fig. 2. Calibration curves for 6-mm truncated edge length tungsten carbide cubes. The calibrations were performed at room temperature (~25 °C) using the three Bi transitions and at 1200 °C using the transitions coesite to stishovite and forsterite to β-spinel transitions. Tons of force was calculated from the oil pressure on a 16-in. ram.

medium consisted of a fired castable MgO-Al_2O_3-SiO_2-based ceramic [compound 584 made to old F100 batch specifications ($CaCO_3$-free, sieved MgO), Aremco Co.] with integral gaskets. Initially, a hole with an outside diameter of 3.175 mm was drilled from face to face through the octahedron and lined with Re foil, which served as a heater. Brucite (~20 mg) was loaded either into a hard alumina annulus (2 mm long), or directly in contact with the heater on top of an MgO filler rod (2.5 mm long). This initial setup proved highly unsatisfactory, however, because the brucite reacted with the alumina annulus and formed Mg-Al spinel. Even in the experiments without the alumina, SiO_2 and Al_2O_3 from the octahedron were found to diffuse through small slits in the Re foil and contaminate the sample. To preserve sample purity a different strategy was needed.

The experimental setup was modified so that a hole with a 4.690-mm o.d. was drilled in the octahedron and lined with a tube 1.520 mm thick of high-purity MgO, which was then lined with Re foil. The alumina annulus was discarded. The MgO liner prevented the pressure medium from contaminating the sample. For quenching experiments, one thermocouple was introduced into the sample region. This thermocouple was inserted into the center of the furnace by drilling a small hole from one equatorial fin to the opposite equatorial fin. This setup had the advantage that the thermocouple bead was buried directly in brucite. For DTA experiments, a second thermocouple was added by slitting the Re foil at the top of the heater and inserting the thermocouple there. All thermocouple leads were electrically insulated from the heater by MgO ceramic sleeves. No correction was made for the effect of pressure on the emf generated. The two multianvil configurations are shown in Figure 1.

After loading the pressure medium, the gasketing fins were wrapped with Teflon tape, and then the octahedron was surrounded by eight tungsten carbide cubes (2.54 cm) with either 6- or 8-mm truncated edge lengths (TEL). The stack of cubes was held together by gluing G10 plastic sheets to the backs of the cubes. Cu strips were inserted into the plastic to serve as electrodes to the cubes in contact with the Re foil. This setup was loaded into the multianvil device and pressurized. Many of the experimental details are described more fully in Walker et al. (1990) and Walker (1991).

Experiments below 12 GPa were slowly pumped to pressure (~8 h to reach 12 GPa), and then heated to temperature. Experiments above 12 GPa were pumped to 9 GPa, heated to 500 °C, pumped to the desired pressure, and then raised to the desired temperature. This two-step pumping procedure greatly reduced carbide loss resulting from blowouts. The 6-mm TEL octahedra were calibrated at room temperature using the Bi I-II, Bi II-III, and Bi III-V transitions. At 1200 °C, calibrations were performed at 9.3 GPa using the coesite to stishovite transition, and at 14.3 GPa using the forsterite to β-spinel transition. The 8-mm TEL octahedra were calibrated similarly up to the coesite-stishovite transition. These fixed points yield the force (tons) vs. sample pressure (GPa) curves in Figure 2. The most critical high-pressure calibration experiments were performed using the experimental setup shown in Figure 1B.

In DTA experiments, the differential signal was recorded on an analogue chart recorder and interfaced to a personal computer. Considerable care was required to condition the signal and filter electrical noise. In the DTA experiments, temperature was raised and lowered in 25–30° steps either by controlling the cold thermocouple or by increasing and decreasing furnace power. In the quenching experiments, samples were brought to the desired pressure and temperature, held there for 30 min, and then quenched by shutting off furnace power. Decompression for both types of experiments was accomplished over the course of about 12–24 h depending on the pressure achieved.

After quench, the entire octahedron was mounted in

TABLE 1. Summary of experiments

DTA experiments							Cook and quench experiments						
Expt.	Type	TEL (nm)	*P* (GPa)	*T* (°C)	Comments	Heating/cooling rate	Expt.	Type	TEL (nm)	*P* (GPa)	*T* (°C)	Comments	*t* (min)
PC 4	PC	—	1.0	782	±5°	100–300 °C/min	223	MA	6	4.0	1050	brucite (Pt capsule)	30
PC 4	PC	—	1.5	930	±5°	100–300 °C/min	218	MA	6	4.0	1020	periclase	30
PC 5	PC	—	2.0	984	±7°	100–300 °C/min	217	MA	6	4.0	1050	periclase	30
PC 7	PC	—	3.0	1076	±5°	100–300 °C/min	215	MA	6	4.0	1100	periclase	20
PC 7	PC	—	4.0	1120	±10°	100–300 °C/min	219	MA	6	6.0	1120	brucite	30
168	MA	8	6.0	1169	±12° (1157–1181°)	100–300 °C/min	206	MA	6	6.0	1140	brucite/periclase	30
121	MA	8	8.0	1191	±19° (1172–1210°)	100–300 °C/min	205	MA	6	6.0	1160	periclase	30
123	MA	8	10.0	1186	±12° (1174–1198°)	100–300 °C/min	204	MA	6	6.0	1200	periclase	30
162	MA	6	11.5	1120	±19° (1101–1138°)	100–300 °C/min	174	MA	6	8.0	1170	brucite	20
							198	MA	6	8.0	1200	periclase	30
							179	MA	6	8.0	1225	periclase	30
							184	MA	6	11.5	1170	brucite	30
							196	MA	6	11.5	1200	brucite/periclase	30
							190	MA	6	11.5	1225	periclase	10
							197	MA	6	13.0	1200	brucite	30
							203	MA	6	13.0	1225	brucite	30
							210	MA	6	13.0	1250	periclase	20
							208	MA	6	13.0	1275	periclase	30
							214	MA	6	15.0	1250	brucite	30
							224	MA	6	15.0	1280	periclase	30

Note: PC = piston cylinder; MA = multianvil.

epoxy, cut in half longitudinally to expose the sample, and polished. The polished sections were examined in reflected light and with backscattered electron imaging using an electron microprobe. Qualitative analyses were sufficient to reveal if the sample remained uncontaminated, and to distinguish brucite from periclase; peak MgO counts are lower for brucite than for periclase.

RESULTS

The results of both DTA and quenching experiments are summarized in Table 1. The dehydration of brucite to periclase and H_2O is an endothermic reaction, and thus a small negative dip was observed in the differential trace as the phase boundary was crossed with increasing temperature in DTA experiments. An example of this type of signal is shown (Fig. 3). As the temperature was increased in successive small increments, the differential temperature normally had a slight positive slope (Fig. 3a); this behavior is contrasted with the pronounced negative slope that occurs when the reaction boundary is passed (Fig. 3b). DTA experiments were carried out to 11.5 GPa, and the results are shown (Fig. 4). The theoretical phase boundary calculated using available thermodynamic data and molecular dynamics to constrain the *PVT* properties of H_2O is also plotted in Figure 4 (S. Saxena, personal communication; Johnson et al., 1991).

The brucite dehydration curve is controversial at low pressures, and many different sets of experiments have resulted in many different curves. Therefore, the DTA results needed to be confirmed by a second independent method. Several different approaches were tried. For example, another in situ method based on a resistance change was tried. The mixture of periclase and H_2O was reasoned to be more conductive than brucite, and therefore, if the resistance across the charge could be monitored, it might be possible to detect that phase change by a sudden change in resistance. Unfortunately, the thermocouple ceramics become semiconductors at high pressures and temperatures, and reliable resistance measurements were not obtained.

After further in situ attempts were abandoned, a nonstandard type of quenching experiment was tried. Given the rapid kinetics of the periclase hydration reaction (both at high temperature, facilitating DTA experiments, and at low temperature, facilitating brucite synthesis) interpreting the appearance of quenched experiments may be difficult because of possible quench modifications. Thus, an experiment designed to produce textural features that might ineradicably record the state of the charge at *P* and *T* rather than during the subsequent quench became a priority. Therefore, a homogeneous 5:1 mix of brucite to zirconia was prepared. Inert zirconia should not affect the brucite dehydration temperature, and it should not participate in any quench reactions. Initially, the zirconia and brucite were well mixed. When the phase transition occurred, the zirconia grains would no longer be supported in a solid matrix; gravity would then cause them to settle to the bottom of the charge. After an experiment was held at pressure and temperature, optical examination would reveal either a marker layer of zirconia at the bottom of the charge, indicating periclase and H_2O had been stable, or the zirconia would still be homogeneously distributed, indicating brucite had remained stable. In practice, although the fluid makes up 50 mol% of the charge after breakdown, the zirconia grains did not settle out of suspension. Evidently, the periclase still formed a self-supporting network, or the fluid was too viscous for settling to occur, or the zirconia crystal distribution was controlled by factors in addition to gravity.

Figure 5A is a backscattered electron image of a section

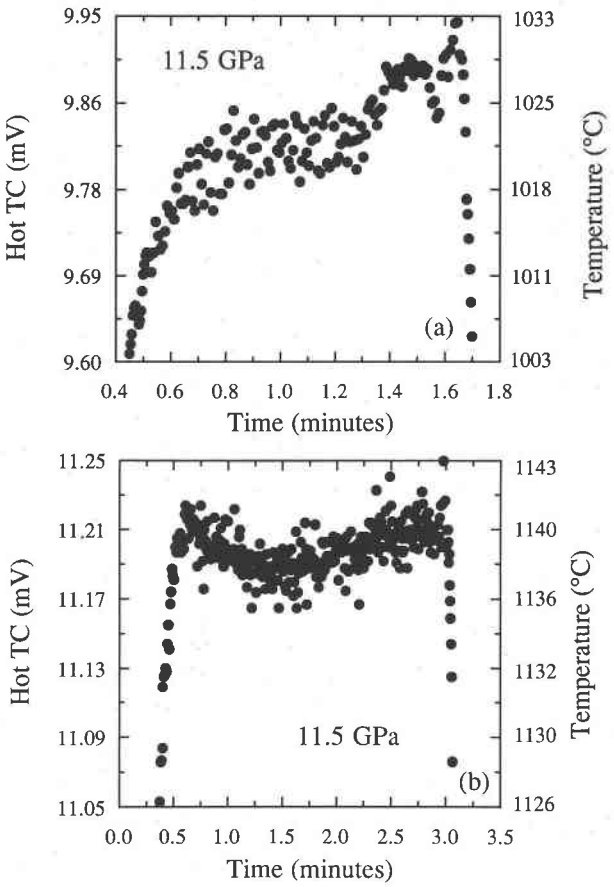

Fig. 3. Trace of the DTA signal recorded at 11.5 GPa. (**a**) This trace shows the normal slightly positive slope of the hot thermocouple as the power is increased in small steps. (**b**) This trace shows a negative slope and signals that the dehydration boundary has been crossed.

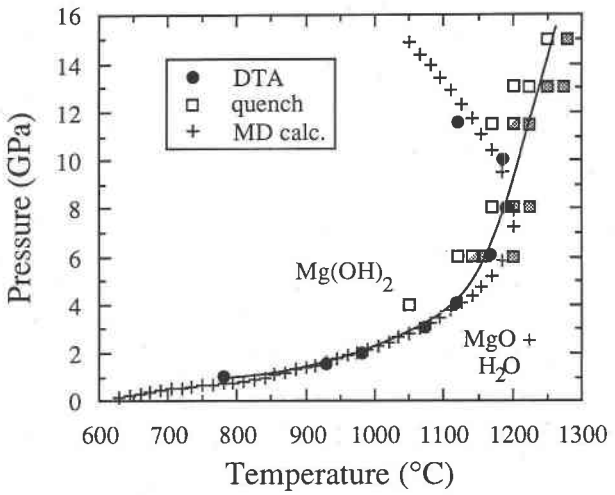

Fig. 4. Experimentally determined phase diagram for the dehydration of brucite to periclase and H_2O. Circles represent the data determined using DTA. Squares represent the data determined using quenching experiments; open squares indicate brucite was stable, stippled squares indicate periclase was stable, and half-stippled squares represent temperatures at which both brucite and periclase were stable. The plus signs are a theoretical phase boundary calculated using molecular dynamics.

of a mixed brucite and zirconia charge quenched after 30 min at 11.5 GPa and 1225 °C (at the thermocouple junction). The sample is much larger than in the DTA experiments and was in a substantial temperature gradient. Theoretically, the isotherms should display an hourglass configuration about the charge's center of thermal symmetry. From the saddle point at the center of the hourglass, isotherms of increasing temperature should approach the inner walls of the Re heater, and isotherms of decreasing temperature should recede along the heater axis. An hourglass pattern is obvious in the zirconia crystal distribution (light speckles), which are slightly concentrated beyond their initial abundance in an X-shaped region. The hot equatorial fields between the arms of the X near the heater walls are occupied by aggregates of zirconia-free brucite platelets with a material of low atomic number (presumably H_2O-rich) in the interstices. The polar fields along the heater axis between the arms of the X are occupied by rather densely compacted periclase (and zirconia), with some interstitial brucite. The thermocouple junction is visible in the upper of these regions. The initial zirconia crystal abundance may be judged from its concentration in the unreacted brucite preserved at the cold ends of the heater beyond these compacted periclase masses. Clearly, the zirconia crystal distribution appears to be controlled more strongly by the thermal structure of the charge than by gravity.

The brucite and periclase distributions, with or without zirconia crystal concentrations, are also related to the thermal structure of the charge. Mass diffusion caused by solubility variation within this temperature gradient most reasonably explains the compaction of periclase within its complementary fluid once brucite broke down. The thermal compaction process in a solubility gradient has been described in detail for silicate systems by Walker et al. (1988) and Lesher and Walker (1988). Buchwald et al. (1985) coined the name thermal migration from observations of the process in metal alloy systems. Within the fluid + periclase aggregate initially produced by brucite dehydration, H_2O diffuses toward the hottest parts of the charge, while MgO diffuses along the periclase solubility gradient toward the coldest regions that are still above the brucite stability temperature. This tendency causes fluid to accumulate along the furnace walls and periclase to compact along an interface, with stable brucite at both ends of the charge. (This process occurs independently of the Soret effect, if it exists, within the fluid. The Soret effect can be an additional agent of mass transport and may either reinforce or inhibit the solubility-induced mass flux.) The periclase that fully compacts by thermal migration expels vapor to the hotter parts of the charge and quenches as periclase; since this periclase is no longer in contact with vapor, it does not fully rehydrate to brucite upon quench. The narrow channels between periclase

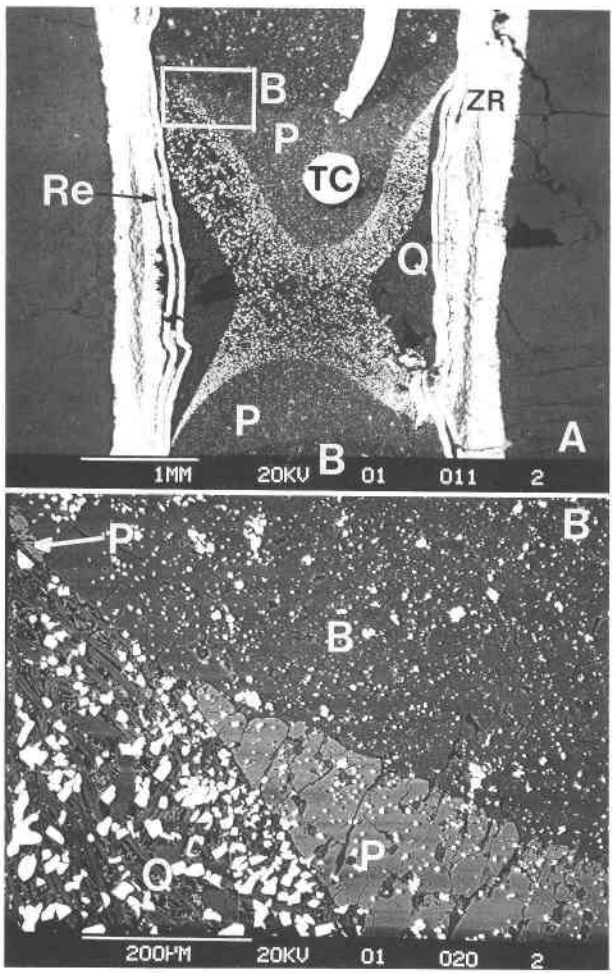

Fig. 5. Backscattered electron image of an experimental charge heated to 1225 °C at 11.5 GPa for 30 min. (**A**) View of the entire charge showing zirconia liner (ZR) between Re-foil heater (Re) and ceramic octahedron, thermocouple junction (TC), quenched brucite platelets (Q), compacted periclase (P), and stable brucite (B). White grains are zirconia crystals. The symmetrical hourglass shape of the labeled fields is controlled by the thermal structure of the charge. Scale bar is 1 mm. (**B**) Close up of box in **A** clearly showing a triple junction among stable brucite (B), compacted periclase (P), and quenched brucite platelets (Q). Note the lens of periclase at upper left of picture. This triple junction represents a thermal erosion front produced during quenching. Scale bar is 200 μm.

grains are filled with finegrained brucite and are interpreted as the entry points for rehydrating the compacted periclase along grain boundaries upon quench. Also upon quench, the fluid pocket reverts to slender brucite platelets with very different morphologies from the equant brucite crystals observed in the cold ends of the charge. This morphological difference is partly related to quench growth from a fluid, in contrast to solid-state recrystallization of the unreacted brucite. But the morphological difference of the area labeled Q (quench brucite) is also tied to the H_2O-rich interstitial material. Because not all the periclase rehydrates, these regions must contain more H_2O than the brucite composition to preserve mass balance.

Thus, although the zirconia-brucite experiments did not work as expected, they demonstrated that the process of thermal compaction creates textural markers that are not fully eradicated upon quench. Thus, the aspect of the thermal gradient that leads to periclase preservation is advantageous, but it also emphasizes that it is important to observe whether compacted periclase or brucite is in contact with the thermocouple bead. This region is the only one where the temperature is well known. The presence of brucite or periclase in other regions of the charge is ambiguous because the temperature at other regions is poorly known. Exploiting the thermal gradient in this fashion greatly simplifies the task of interpreting whether periclase and H_2O or brucite had been stable at peak temperature and pressure.

The inference that vapor and periclase can react to produce brucite on quench is reinforced by an additional textural aspect of this experiment. The thermocouple bead is clearly in a field of compacted periclase (Fig. 5A). The interesting feature of this texture, however, is that a triple junction exists among equant brucite crystals, compacted periclase, and brucite platelets (Fig. 5B). This geometry cannot be an equilibrium phenomenon because it implies crossing isotherms. Equant brucite, compacted periclase, and brucite platelets are features that form at increasingly higher temperatures, and no temperature exists where all three can be stable.

Since this geometry cannot be an equilibrium feature, it must have formed on the quench. We infer that a layer of compacted periclase existed at equilibrium along the interface with the stable brucite crystals; this layer is present in the three other corners of the charge (Fig. 5A). Indeed, a small lens of compacted periclase is still present at the upper left corner of this interface (Fig. 5B). During quench, this periclase layer was thermally eroded by reacting with the adjacent vapor and rehydrating to brucite platelets. The inference that rapid brucite regrowth is possible during quench is strengthened by the observation that brucite was synthesized very easily from periclase and H_2O at only 225 °C. Although the temperature falls quickly (~5 s) from peak temperature to 100 °C, the thermal inertia of the wedges and cubes keeps the temperature at ~100 °C for 3 or 4 min. We suspect that some of the thermal erosion may occur at these low temperatures rather than strictly during the high-temperature quench.

Figure 6A and 6B illustrates the symmetrical distribution of unrecrystallized brucite, compacted periclase, and quenched fluid (now brucite platelets and interstitial H_2O-rich material) without the additional complications of the zirconia crystal distribution. Clearly, the compacted periclase has suffered substantial rehydration, as shown in the detail of Figure 6B. Because the thermocouple junction is not in the unrecrystallized brucite field, we interpret this experiment's pressure and thermocouple temperature as being in the periclase + fluid field. We

address below the issue of whether this fluid is a vapor or a melt.

The results of the quenching experiments interpreted using the above guidelines are shown in Figure 4. The DTA and quenching curves agree fairly well to 10 GPa but diverge quite rapidly at higher pressures. Most importantly, the unique change from positive to negative slope predicted by molecular dynamics and corroborated by the DTA experiments (Johnson et al., 1991) was not confirmed.

Discussion

Experimental difficulties

The discrepancy in the DTA and quenching results at 11.5 GPa requires an explanation. After the experiment, careful analysis of the DTA charges using backscattered electron imaging revealed that these samples suffered from fluid phase contamination. Specifically, SiO_2 and Al_2O_3 peaks, as well as MgO peaks, were observed by energy-dispersive X-ray analysis in the fluid-rich regions of these charges. The source of the SiO_2 and Al_2O_3 is the surrounding octahedral pressure medium. Evidently, these oxides could invade the sample region through microscopic slits in the Re foil heaters, possibly by leaching when H_2O was formed from brucite dehydration.

The contamination of these experiments by the pressure medium makes the DTA results suspect. Since SiO_2 and Al_2O_3 dissolve in the fluid phase, they lower the Gibbs free energy of the fluid and artificially increase its stability field; fluid phase contamination, therefore, will cause brucite to dehydrate at a lower temperature than in the uncontaminated case. Because the DTA and quenching results agree very nearly to about 10 GPa, the contamination problems appear to become severe at pressures greater than 10 GPa. This observation could mean that the fluid phase solubility of SiO_2 and Al_2O_3 increases at 10 GPa. The piston-cylinder experiments were conducted in sealed Pt capsules and thus did not suffer from contamination problems. The quenching experiments did not suffer from contamination because the MgO liner isolated the pressure medium from the charge. The quenching results above 10 GPa are believed to be more accurate than the DTA results because they are uncontaminated and thermal migration allowed the results to be interpreted reliably. These quenching experiments are assumed to define the brucite breakdown curve at high pressures most accurately.

We infer that brucite breaks down by dehydrating at all pressures studied. If a melting curve was intersected at some pressure, then the reaction would change (e.g., Ellis and Wyllie, 1979). By analogy with other hydrous minerals, the most likely melting reaction to intersect would be $Mg(OH)_2 \leftrightarrow MgO$ + melt. One possible explanation of the slope change initially signaled by the DTA results was that an invariant point was reached, and the breakdown changed from a dehydration reaction to a melting reaction. The quenching results, however, show

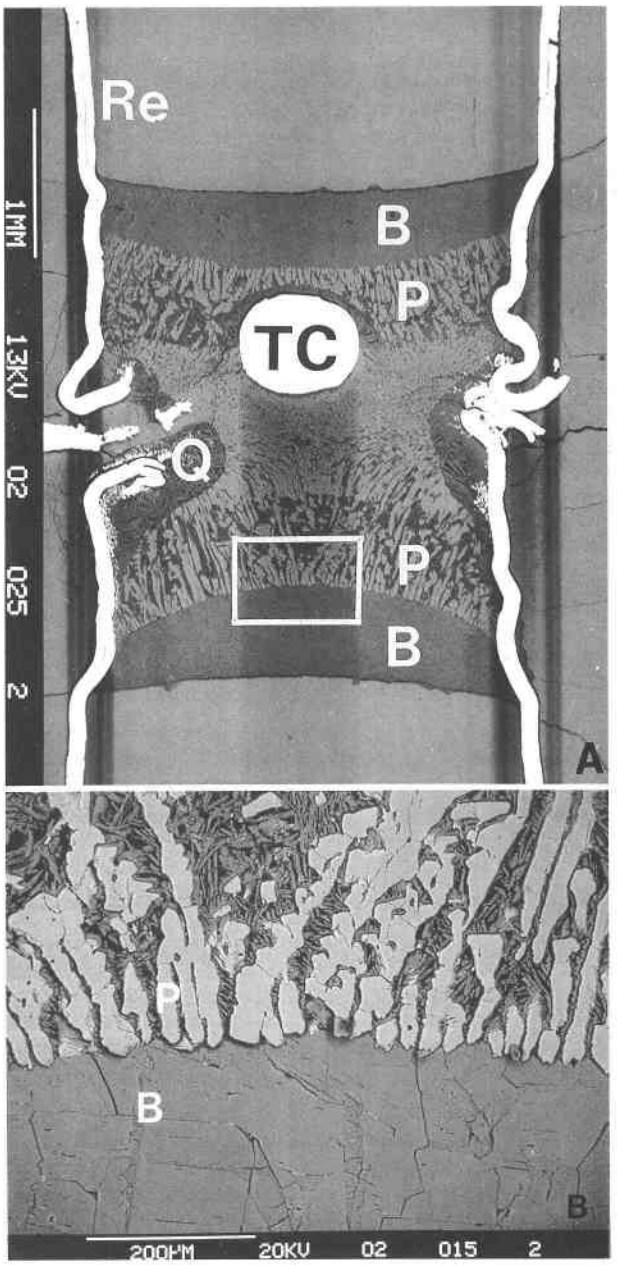

Fig. 6. Backscattered electron image of an experimental charge pressurized to 13 GPa and heated to 1250 °C for 20 min. (**A**) View of the entire charge showing Re-foil furnace (Re), thermocouple junction (TC), quenched brucite platelets (Q), compacted periclase (P), and stable brucite (B). The TC junction is entirely outside the field of stable brucite crystals. The horizontal gray stripe of material in the middle of the charge directly below the TC junction is partly MgO thermocouple insulation. Scale bar is 1 mm. (**B**) A close up of the interface between compacting periclase and stable brucite (box in **A**). Contrast the feathery quench brucite crystals between the lenses of periclase to the equant brucite crystals in the fields labeled B. Scale bar is 200 μm.

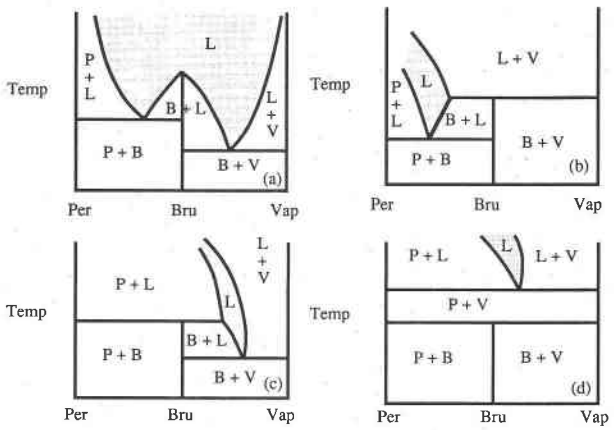

Fig. 7. Four possible topologies representing how brucite can break down at high temperatures and pressures. (**a**) Brucite melts congruently. (**b**) Brucite melts to an MgO-rich liquid. (**c**) Brucite melts to an MgO-poor liquid. (**d**) Brucite dehydrates to periclase and vapor, which melt at a higher temperature. The experimental results suggest that topologies **a**, **b**, and **c** are incorrect.

no discontinuity in slope at these pressures, making this explanation less likely. Indeed, one smooth curve can be fitted to both the low-pressure DTA data points and the high-pressure quenching results, implying that the reaction is continuous from 1 to 15 GPa. The possibility of a melting reaction was investigated experimentally, however.

Theoretically, brucite must break down in one of four ways (Fig. 7). If brucite melts congruently (Fig. 7a) or if brucite breaks down to produce a very MgO-rich liquid (Fig. 7b), then a brucite bulk composition cannot produce periclase as an end product of the initial decomposition. Since periclase is observed as an end product in many experiments, these two constructions must be topologically incorrect. Two possibilities remain; either brucite breaks down by melting to form an MgO-poor liquid (Fig. 7c), or it breaks down by dehydrating (Fig. 7d). A brucite bulk composition produces periclase plus fluid in either case, and these two topologies are texturally indistinguishable.

To differentiate between these two possible topologies, a more H_2O-rich composition than brucite (38 mg of brucite and 72 mg of distilled, deionized H_2O) was loaded into a Pt capsule, which was sealed on both ends. The capsule was held in a large Cu heat sink during welding in order to keep most of the capsule at a temperature below the boiling point of H_2O. Some Pt was observed to spall off during welding, so the mol% H_2O remaining in the capsule after welding was calculated in two ways. For the best case, the weight difference measured before and after welding was all attributed to Pt loss. For the worst case, the weight difference was all attributed to H_2O loss. The two calculations yield 82 and 68 mol% H_2O, respectively. This capsule was then brought to 11.5 GPa and 1225 °C, a pressure at which the DTA curve shows a change in slope at lower temperature, and held at these conditions for 30 min.

If brucite breaks down by melting at this pressure and temperature and our bulk composition lies to the right of the liquid composition, then an MgO-poor liquid and a H_2O-rich fluid will be generated (Fig. 7c). If brucite breaks down by melting and our bulk composition is to the left of the MgO-poor liquid composition (but more H_2O-rich than a brucite bulk composition alone), we will be either in the brucite + liquid stability field or in the periclase + liquid stability field. Since we are at a temperature only 25 °C above the stable brucite field at this pressure, we suggest that we are most likely to encounter the brucite + liquid stability field. In either of these cases, upon quench the fluid + liquid or brucite + liquid will revert to brucite. Periclase will not be observed as an end product. On the other hand, if brucite breaks down at this pressure and temperature by dehydrating, then a brucite + H_2O bulk composition will generate a H_2O-rich fluid and periclase (Fig. 7d). The periclase will compact towards the cold end of the charge, and, although the fluid will revert to brucite upon quench, some of the compacted periclase will quench as periclase. This scenario is the only one in which periclase will be observed as an end product. The experimental charge was sectioned and polished after being held at P and T, and periclase and quenched brucite were observed. This experiment coupled with the continuous nature of the reaction curve suggests that, to at least these pressures and temperatures, brucite breaks down by dehydrating; a melting reaction does not appear to intersect the dehydration curve. This interpretation is in contrast to the recent study of Gasparik and Zhang (1992), who state that brucite appears to melt incongruently between 12 and 22 GPa at 1250 °C.

Comparison with previous results

Previous experimental results on brucite stability at pressures above 1 GPa are compared with the present results (Fig. 8). The low pressure results agree well with Irving et al. (1977) and do not reproduce the change in slope observed by Yamaoka et al. (1970) at ~3 GPa and 1000 °C. The new results indicate that the brucite dehydration curve is at a higher temperature than that reported by Kanzaki (1991) and do not confirm the change in slope at about 6–7 GPa observed by Leinenweber et al. (1991) using in situ X-rays. One difference between this study and the two recent studies is the thermocouple type used. Pt-Pt/Rh thermocouples were used in this study, whereas Kanzaki (1990, 1991) and Leinenweber et al. (1991) used W-Re thermocouples. All the reported temperatures are uncorrected for a pressure effect on the thermal emf. The pressure effect correction is different for each thermocouple type because the Seebeck coefficients vary uniquely with high pressure. Although absolute pressure corrections have not been determined, relative pressure corrections for W-Re and Pt-Pt/Rh thermocouples have been observed (Williams and Kennedy, 1969; Ohtani, 1979). These corrections indicate that

both thermocouples record lower temperatures than ambient at high pressure, but that the pressure effect on W-Re thermocouples is less severe. Therefore, qualitatively correcting for an emf pressure effect would raise all the reported temperatures but would raise the Pt-Pt/Rh temperatures more than the W-Re temperatures at the temperatures considered here (<1300 °C). This correction would increase rather than decrease the difference in results.

Experimental studies can be plagued by many different problems. Two problems that were experienced during this study are fluid phase contamination and loss of H_2O leading to P_{H_2O} less than P_{tot}. Fluid phase contamination was avoided in later experiments by using an MgO liner and pure MgO thermocouple insulators. H_2O leakage was avoided in the piston-cylinder experiments by using sealed Pt capsules. At pressures greater than 6 GPa, we infer that H_2O-vapor did not completely leak from the experimental assemblies because periclase easily rehydrated to brucite upon quench in the hottest regions of the charge. For this reaction to occur, H_2O must have been present at the end of the experiment. As argued above, this H_2O was present as a vapor rather than dissolved in a melt phase. The presence of an H_2O-vapor at the experiment's conclusion guarantees that P_{H_2O} remained equal to P_{tot} at pressure and temperature, even if slight H_2-diffusion occurred during the experiment. This observation suggests that at these very high pressures, no cracks or voids exist that allow H_2O to escape from the charge. H_2O may only leak from the experiment by diffusing through the Re foil heater and the MgO liner. The short experimental times (30 min) prevented this process from proceeding to completion. Thus, the Re foil and MgO end pieces served as physically sealed capsules for these experiments, although it is unlikely that H_2 diffusion through these materials was entirely inhibited.

Our results at 6 GPa and higher pressures are contrasted with our quenching results at 4 GPa. Experiments conducted at 4 GPa using identical procedures as in the high-pressure experiments consistently yielded periclase even at temperatures well within the brucite stability field, as inferred from our 4-GPa DTA experiment. A notable difference between these 4-GPa quenching experiments and the 6-GPa quenching experiments is that no vapor field (quench brucite field) was observed in any of the 4-GPa experiments. Secondly, a small portion of the MgO liner hydrated to brucite in some of the 4-GPa experiments. These two observations imply that H_2O had leaked from the sample region, but it had not traveled far. It merely reacted with the MgO liner, which was at a slightly lower temperature, to form brucite. Therefore, the presence of periclase at experiments well within the predicted brucite field must be attributed to a loss of H_2O, which allowed P_{H_2O} to become less than P_{tot}. This condition causes brucite to dehydrate at lower temperatures than when $P_{H_2O} = P_{tot}$. This suggestion was tested by conducting an experiment at similar conditions but loading the brucite into a sealed Pt capsule. This experiment yielded stable brucite

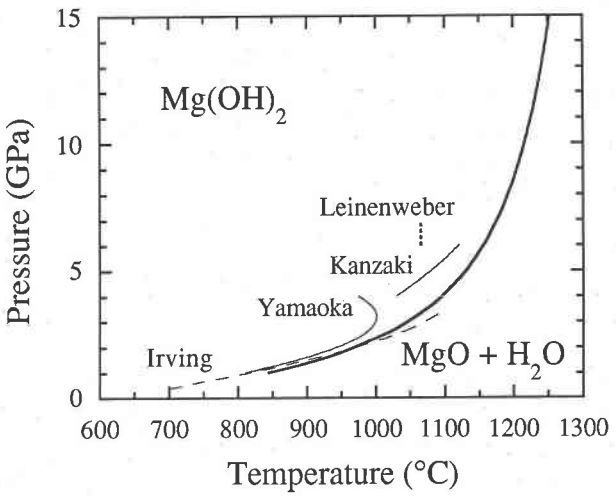

Fig. 8. Comparison of the new data with previous experimental studies of brucite stability conducted at pressures above 1 GPa. The new data are shown by the thick unlabeled curve. Previous data are from Yamaoka et al. (1970), Irving et al. (1977), Kanzaki (1991), and Leinenweber et al. (1991). The new data show the highest thermal stability for brucite and are believed to be the least subject to experimental error.

consistent with our explanation and the high pressure experiments. The difference in H_2O leakage rates between 4 and 6 GPa implies that a void in the octahedral pressure medium is not completely sealed off at the low tonnage required to reach 4 GPa but is sealed off by 6 GPa.

The differing results in our quenching experiments at 4 and 6 GPa combined with the recognition of fluid phase contamination clearly demonstrate that the periclase and fluid stability field can be markedly overestimated. This lesson may apply to the experiments of others as well. An additional problem in multianvil experiments is the offset between the sample and the thermocouple bead. If the sample is located in the hot spot, but the thermocouple is displaced from the sample, the thermocouple will record a temperature lower than the sample temperature. We avoided this problem by surrounding the thermocouple bead with brucite and then observing whether brucite or compacted periclase was present immediately adjacent to this junction. Experiments conducted at identical pressures but above the breakdown temperatures reported by Kanzaki (1990, 1991) and Leinenweber et al. (1991) yield euhedral brucite crystals, indicating that brucite is stable at these temperatures. These new results are inconsistent with the previous findings. The only problem that could cause brucite stability to be overestimated in our experiments is lack of recognition of brucite formed on quench from rehydrated periclase. Rehydrated periclase was easily recognized in this study because of the action of thermal migration. All of the difficulties discussed above would lead to underestimation of the brucite stability field. Because our data show the highest temperature brucite stability field for any given pressure, we argue that our

experimental data are the least subject to the types of errors just described. These new data most accurately record brucite dehydration temperatures.

Thermodynamic calculations

The objective of this work was to determine the brucite dehydration curve to 15 GPa and then use these new phase equilibria data to calculate the volume (density) of H_2O at mantle pressures. Brucite dehydration appeared to be a particularly appropriate reaction to study because the P-T slope was predicted to change from positive to negative. This slope change would allow the molar volume of H_2O to be calculated very accurately at the temperature maximum. The Clausius-Clapeyron equation requires that for some special univariant equilibria, the P-T curve is a function of the differences in entropies and volumes of the solids and reactants:

$$\frac{dP}{dT} = \frac{\Delta S}{\Delta V}. \tag{1}$$

If the P-T curve shows a maximum temperature, then the slope is infinite, and $\Delta V = 0$ at this maximum. Therefore, the molar volume of H_2O at this pressure and temperature is exactly equal to the difference in volumes of periclase and brucite; the entropies at pressure and temperature of brucite, periclase, and H_2O are irrelevant. Because only molar volumes need to be calculated, errors associated with the thermochemical data are not introduced.

The experimental data, however, indicate that the slope remains positive to 15 GPa. Since the entropies of brucite, periclase, and H_2O are not well-known functions of temperature and pressure, the molar volume of H_2O along the dehydration curve was calculated using the equation

$$\begin{aligned}\Delta G(P, T) = 0 \\ = \Delta H^0_T - T\Delta S^0_T + \int_{1\text{ bar}}^{P} \Delta V_s(P, T)\, dP \\ + \int_{1\text{ bar}}^{P} V_f(P, T)\, dP\end{aligned} \tag{2}$$

where ΔH^0_T and ΔS^0_T are the enthalpy and entropy changes for the reaction at 1 bar and temperature T, ΔV_s equals the volume change in the solid phases, and V_f is the fluid volume. Note that Equation 2 has been written so that the only unknown quantity is the last term on the RHS.

In Equation 2, ΔS^0_T and ΔH^0_T are defined as

$$\Delta S^0_T = \Delta S^0_{298} + \int_{298}^{T} \frac{\Delta C_P}{T}\, dT \tag{3}$$

$$\Delta H^0_T = \Delta H^0_{298} + \int_{298}^{T} \Delta C_P\, dT. \tag{4}$$

The volume integrals for the solids were solved using the Murnaghan equation

$$V(P, T) = V(1\text{ bar}, T)\left[1 + \frac{k'_0 P}{k_0}\right]^{-1/k'_0} \tag{5}$$

where $V(1\text{ bar}, T)$ follows directly from the definition of thermal expansion as

$$\begin{aligned}V(1\text{ bar}, T) \\ = V_0 \exp \int_{298}^{T} \alpha(T)\, dT \\ = V_0 \exp\left[a_0 T + \frac{a_1(T^2)}{2} + a_2 \ln T - \frac{a_3}{T}\right]\Bigg|_{298}^{T}.\end{aligned} \tag{6}$$

In Equations 5 and 6, k_0 is the bulk modulus, k'_0 is the pressure derivative of the bulk modulus, V_0 is the molar volume at 1 bar, 298 K, and $\alpha(T)$ is the thermal expansion. The constants a_0, a_1, a_2, a_3 are determined by regressing experimental data. Evaluating this integral for, say, periclase gives

$$\begin{aligned}\int_{1\text{ bar}}^{P} V_{per}(P, T)\, dP \\ = V(1\text{ bar}, T)\left(\frac{k_0}{k'_0 - 1}\right)\left[\left(1 + \frac{k'_0 P}{k_0}\right)^{(1 - 1/k'_0)} - 1\right].\end{aligned} \tag{7}$$

The bulk modulus (or compressibility) was treated as an explicit function of temperature following Saxena (1989). Thermodynamic constants and the sources where these constants were obtained are listed in Table 2. The volume derivatives α and β in Table 2 are corrected for misprints in the published versions (S. Saxena, 1992 personal communication) and are based upon optimized fits of a variety of low-pressure phase equilibria data involving these phases.

Equation 2 is valid only along the univariant curve. Therefore, the new experimental data were fit with a smooth curve determined by minimizing the residuals in a least-squares sense. To facilitate constraining the curve accurately at low pressures, the experimental data of Barnes and Ernst (1963), Schramke et al. (1982), and Irving et al. (1977) were included, along with the new data of this study in the fitting procedure. The form of this fitted curve is not intended to have thermodynamic significance; it merely allows the dehydration curve to be manipulated mathematically. The equation for the fitted curve (P in GPa, T in °C) is

$$T = 1307 + 1.154P - \frac{1192}{P + 1.576} (r^2 = 0.992). \tag{8}$$

Since little consistent phase equilibrium data exist for this dehydration reaction at pressures below 1 kbar (e.g., compare Barnes and Ernst, 1963, vs. Weber and Roy, 1965, vs. Bowen and Tuttle, 1949), the volume integral of H_2O (or $RT \ln f_{H_2O}$) from 1 bar to 1 kbar was computed using the modified Redlich-Kwong model of Kerrick and Jacobs (1981). This modification was incorporated into Equation 2 by making the following changes:

TABLE 2. Thermodynamic properties

Phase	V_0 (cm³/mol)	ΔH^0_{298} (kJ/mol)	ΔS^0_{298} (kJ/mol/K)	k'_0				Ref.*
Brucite	24.630	−925.500	64.40	4.712				R, H, S
Periclase	11.250	−601.490	26.94	4.170				R, J
H_2O	—	−241.814	188.83	—				R
		$\alpha(T)(K^{-1}) = a + bT + c/T + d/T^2$						
	$a(\times 10^{-5})$	$b(\times 10^{-8})$	$c(\times 10^{-2})$	$d(\times 10^{-1})$				
Brucite	8.754	1.809	−2.218	5.843				S
Periclase	3.754	0.791	0.000	−7.836				SZ
		$\beta(\text{bars}^{-1}) = a + bT + cT^2 + dT^3$						
	$a(\times 10^{-6})$	$b(\times 10^{-11})$	$c(\times 10^{-13})$	$d(\times 10^{-16})$				
Brucite	1.75100	−0.5489	2.04450	1.10500				S
Periclase	0.59506	8.2334	0.32639	0.01018				SZ
		$C_p(\text{J/K}) = a + bT + c/T^2 + dT^2 + e/T^3 + f/T^{0.5} + g/T$						
	a	$b(\times 10^{-2})$	$c(\times 10^6)$	$d(\times 10^{-8})$	$e(\times 10^2)$	f	$g(\times 10^2)$	
Brucite	103.010	1.6533	−2.7462	0.00	−1.365	0.00	−1.141	K
Periclase	43.570	0.5480	−1.6779	−6.31	0.000	0.00	33.390	R
H_2O	46.461	0.5966	6.3200	0.00	−7957000	0.00	−166.300	R

Halbach and Chatterjee (1982) coefficients

$$a(T) = 1.616 \times 10^8 - 4.989 \times 10^4 T - 7.358 \times 10^9/T$$

$$b(P) = \frac{1 + 3.4505 \times 10^{-4}P + 3.8980 \times 10^{-9}P^2 - 2.7756 \times 10^{-15}P^3}{6.3944 \times 10^{-2} + 2.3776 \times 10^{-5}P + 4.5717 \times 10^{-10}P^2}$$

Note: T is measured in degrees Kelvin; P is measured in bars.

* References: R = Robie et al. (1979); H = Holland and Powell (1990); D = Duffy et al. (1991); J = Jackson and Niesler (1982); SZ = Saxena and Zhang (1989); S = Saxena (1989); K = King et al. (1975).

$$\Delta G(P, T) = 0 = \Delta G(1 \text{ kbar}, T) + \int_{1 \text{ kbar}}^{P} \Delta V_s(P, T)\, dP + \int_{1 \text{ kbar}}^{P} V_f(P, T)\, dP \quad (9)$$

where

$$\Delta G(1 \text{ kbar}, T) = \Delta H^0_T - T\Delta S^0_T + \int_{1 \text{ bar}}^{1 \text{ kbar}} \Delta V_s(P, T)\, dP + \int_{1 \text{ bar}}^{1 \text{ kbar}} V_f(P, T)\, dP. \quad (10)$$

The practical effect of computing $\Delta G(P, T)$ from a baseline of 1 kbar rather than the standard 1 bar is that the uncertain and contradictory phase equilibria data that exist below 1 kbar are no longer of interest in computing V_{H_2O} at high pressure on the basis of the phase equilibrium curve. Inasmuch as V_{H_2O} is well known by direct measurement at 1 kbar, we sacrifice little new knowledge by using V_{H_2O} to 1 kbar as input, rather than seeking its recovery as output. Furthermore, the direct measurements of V_{H_2O} from 1 to 10 kbar can still be used to check the calculated volumes in a region where the lowest pressure noise in phase equilibrium determinations has subsided.

The last term on the RHS of Equation 9 can be evaluated as a function of pressure every 200 bars along the P, T of the dehydration curve using Equation 8 and the data in Table 2. Figure 9a illustrates the graphical meaning of this term. Physically, this term is the area under the volume as a function of pressure curve. Since volume is a function of T as well as P, a series of isothermal curves exist on this plot. Therefore, the integral of the volume of H_2O at a particular P and T along the dehydration curve (P_1, T_1) is the area under the $V(P)$ curve for the particular isotherm (T_1) at which P_1 is the equilibrium brucite dehydration pressure. The integral can be formed again at some new P_2, T_2 along the dehydration curve, and a new area under the second curve is identified. If both integrals had been formed at the same T_1, then $V(T_1)$ at the average pressure between P_1 and P_2 can be computed from

$$V_{H_2O}\left(\frac{P_1 + P_2}{2}, T_1\right) = \frac{\int_{1 \text{ kbar}}^{P_2} V(P_2, T_1)\, dP - \int_{1 \text{ kbar}}^{P_1} V(P_1, T_1)\, dP}{(P_2 - P_1)}. \quad (11)$$

In other words, the volume we seek is equal to the difference in the integrals of the volume of H_2O at P_2 and P_1 divided by the difference between P_2 and P_1. Figure 9a shows, however, that the integrals computed from Equation 9 do not bear the required isothermal relationship for V_{H_2O} computation, as a result of the shaded wedge introduced by the covariant change of T with P variation along the dehydration curve. This shaded wedge makes the molar volumes calculated using this approach too large.

Figure 9b presents volume integrals (= $RT \ln f$) of the information in Figure 9a as a function of P. The phase

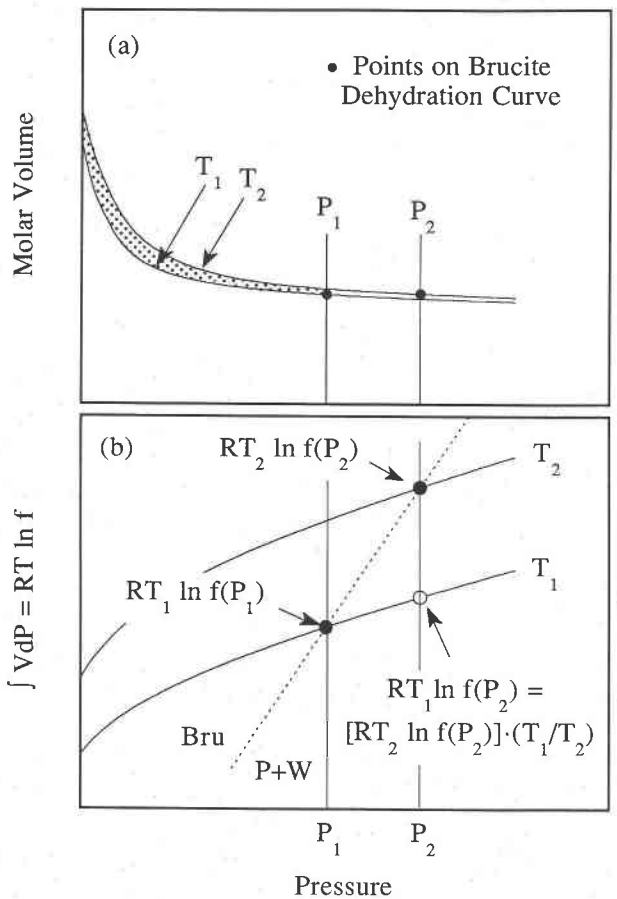

Fig. 9. (**a**) Schematic illustration of molar volume vs. pressure for two isotherms. The volume integral of the fluid in Eq. 9 is physically represented as the area under the curve for some P and T. The shaded region represents the extra volume that is calculated when two successive integrals at different pressures and temperatures are subtracted. (**b**) Schematic illustration of relationship between RT ln f and pressure. To correct for the extra volume of **a**, the term RT_2ln $f(P_2)$ must be reduced by multiplying by T_1/T_2. See text for details.

equilibria allow RT_1ln $f(P_1)$ and RT_2ln $f(P_2)$ to be calculated from Equation 9. However, to use Equation 11 to compute V_{H_2O} at $[(P_1 + P_2)/2, T_1]$, one needs RT_1ln $f(P_2)$. This term is found by multiplying the term we know [namely RT_2ln $f(P_2)$] by a correction factor, T_1/T_2:

$$\int_{1\text{ kbar}}^{P_2} V(P_2, T_1)\,dP = RT_1 \ln f(P_2)$$

$$= [RT_2 \ln f(P_2)]_{\text{Eq. 9}} \cdot \frac{T_1}{T_2}. \quad (12)$$

With this substitution, Equation 11 has been used to compute V_{H_2O} at 200-bar intervals along the brucite dehydration curve to 15 GPa. These results are shown in Figure 10 from 1 to 15 GPa. The calculations give a V_{H_2O} at 1 GPa and 845 °C of 21.3 cm³ compared with the accepted value of 20.8 cm³ from Burnham et al. (1969). This residual error could probably be removed by further parameter optimization. These calculations were repeated using the thermodynamic and volumetric properties of Holland and Powell (1990), which are applicable to 4 GPa. No difference exists in the calculated volume of H_2O to this pressure, and thus further attempts at input parameter selection were deemed unjustified.

Very recently, new physical property data on brucite have become available as experiments have been conducted in a diamond-anvil cell using synchrotron X-ray diffraction to 35 GPa at 300 K and to 80 GPa at 600 K (Yingwei Fei, 1992 personal communication). These experiments are one of the first attempts to measure the thermal expansion coefficient of brucite at 1 bar, the pressure dependence of the thermal expansion, and the temperature derivative of the bulk modulus. These new data were used to define a more accurate equation of state for brucite than was previously possible (Yingwei Fei, 1992 personal communication). The thermodynamic calculations performed above were repeated using these new brucite PVT properties. The calculated molar volume of H_2O changed by less than 1% at 1 GPa and by less than 0.1% at 15 GPa. Although the calculated results changed negligibly, these new volumetric data greatly reduce a possible source of error in our input parameters.

The molar volume of H_2O was also calculated at the same pressures and temperatures using two MRK models (Halbach and Chatterjee, 1982; Kerrick and Jacobs, 1981). The original Redlich Kwong equation is

$$P = \frac{RT}{V - b} - \frac{a}{V(V + b)T^{0.5}}. \quad (13)$$

The two terms on the RHS correct for the repulsive and attractive intermolecular interactions, respectively. Redlich and Kwong (1949) modeled a and b as constants for individual gas species. Modifications of this original equation have involved attempts to parameterize a and b as functions of pressure and temperature. For example, Kerrick and Jacobs (1981) assumed that a is a function of P and T, although b was still treated as a constant (b = 29 for H_2O). However, they modified the repulsive term of Equation 13 to incorporate Carnahan and Starling's (1972) hard sphere model. In contrast, Halbach and Chatterjee described $a(T)$ and $b(P)$ only. A second important difference between these two models is that Kerrick and Jacobs used only the low-pressure PVT data of Burnham et al. (1969) to constrain their parameterizations, whereas Halbach and Chatterjee used low-pressure data in conjunction with super high-pressure shock wave data (i.e., Rice and Walsh, 1957). The Kerrick and Jacobs model is claimed to be accurate to only 2 GPa, whereas Halbach and Chatterjee considered their model to be robust to 1000 °C and 20 GPa. The molar volumes of H_2O calculated using these two MRK equations and the new data calculated from brucite dehydration are compared in Figure 10. The agreement at high pressures between the new calculations and Halbach and Chatterjee's MRK is impressive. In this range of P and T, the molecular

dynamic model of Belonoshko and Saxena (1991) predicts virtually the same volumes as Halbach and Chatterjee's model.

Although the volume of H_2O would appear then to be quite well constrained at high pressure along the dehydration curve, we should point out that this constraint does not imply that the slope of the dehydration curve can be computed with great accuracy. Even though the relative importance of the heat capacity terms is smaller than the volume terms as a consequence of the steep dP/dT slope, the steepness of the slope dictates that ΔV of the reaction is very small. Therefore, small errors in V_{H_2O} can lead to large errors in predicted dehydration curve slope.

Sources of error

Errors associated with the experimentally determined pressures and temperatures were evaluated by fitting dehydration curves with slopes as different as possible, but still consistent with the experimental data. These fitted curves were then used to calculate high-pressure volumes, and the calculated volumes differ by less than 1% at 15 GPa. Therefore, this source of error was considered trivial. Three other major sources of error, however, need to be considered. None of these errors can as yet be evaluated quantitatively.

1. The P-T coordinates determined from the experimental data are subject to error because a correction for the effect of pressure on the thermal emf of S-type thermocouples has not been imposed. An attempt to estimate the magnitude of this correction was made by using the correction factors of Getting and Kennedy (1970). These correction factors are based on experimental data up to 1000 °C and 3.5 GPa. Using the reported polynomial equation and a pressure seal temperature of 150 °C results in a correction factor of ~14 °C at 4 GPa, ~21 °C at 8 GPa, and only 17 °C at 15 GPa. This result does not make physical sense because the magnitude of the pressure correction should increase with increasing pressure. These preliminary calculations confirm that the reported equation cannot be extrapolated with accuracy beyond the 5-GPa limit implied by the authors. Instead, the corrections above 5 GPa were estimated graphically, and they amounted to +60 °C at 15 GPa and 1280 °C. A new smoothed dehydration curve was fitted to these temperature-corrected data. Recalculating molar volumes using this new curve resulted in no change in volume to 6 GPa, and then slightly smaller volumes with increasing pressure (e.g., 10.5 vs. 10.2 cm^3 at 15 GPa). These calculations indicate the size of the error associated with ignoring the pressure effect on emf but cannot be performed quantitatively until more accurate data on this effect at high pressure are available.

2. The molar volumes calculated above assume that the fluid phase is pure H_2O. At these high pressures, however, it is likely that some MgO is dissolved in the fluid. The quantity of MgO dissolved in the fluid is unknown. This dissolved MgO will result in an activity of H_2O less than one, will change the stoichiometry of the equilibrium, and will modify the entropy and enthalpy of the fluid. From the agreement between the calculations presented here for high-pressure H_2O volumes determined from the slope of the dehydration curve vs. the volumes measured from shock waves, the MgO solubility appears to have little effect on fluid volume.

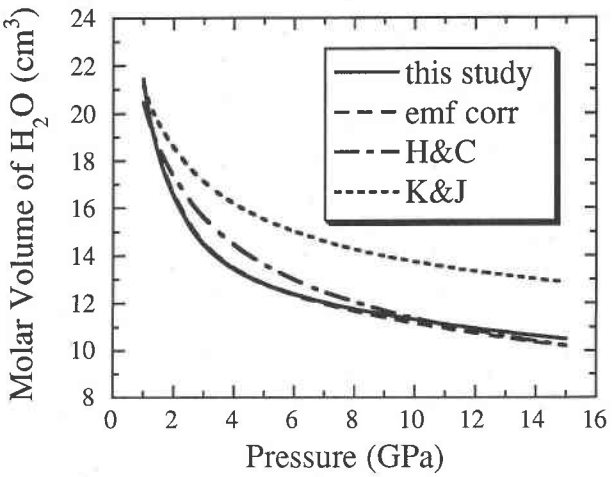

Fig. 10. The molar volume of H_2O calculated using the new phase equilibrium data from 1 to 15 GPa at temperatures along the brucite dehydration curve. These calculated volumes are compared with the volumes calculated using the MRK models of Halbach and Chatterjee (1982; H&C) and Kerrick and Jacobs (1981; K&J). Also shown are the molar volumes calculated by estimating the pressure correction on thermal emf at high pressures.

3. Equation 2 calculates the difference in Gibbs free energy by raising the products and reactants first to temperature and then to pressure. This method of calculating ΔG is only correct if the GPT surface is not curved irregularly; if this surface has curvature, then Equation 2 will result in an erroneous ΔG. The volume integrals are probably the least affected by this assumption because the pressure derivative of the bulk modulus is incorporated into the expressions. This term, k_0', accounts for the curvature of the volume as a function of pressure. The expressions used to evaluate the enthalpy and entropy at high temperature, Equations 3 and 4, however, rely on using the heat capacity at constant pressure. Since the coefficients in Table 2 are derived empirically by linearly regressing 1-bar data, it is possible that the true heat capacity coefficients at 15 GPa are different. It is difficult to estimate how much of a change may occur. However, since the P-T curve is nearly vertical in the range from 6 to 15 GPa, the ΔV term must dominate the ΔS term (Eq. 1). Thus, the significance of errors in the heat capacity coefficients is reduced.

Acknowledgments

We thank Surendra Saxena for initially suggesting this project, for generously allowing us the use of his as yet unpublished optimized thermodynamic and volumetric data, and for advice at various stages. We thank

Yingwei Fei for providing us with his recently acquired brucite volumetric data, and for kindly agreeing to allow us to cite them in this work. We thank Peter McNutt and Teddy Koczynski for technical help and expertise. We thank John Longhi, Dean Presnall, and an anonymous reviewer for thoughtful suggestions, which helped to improve this manuscript. This work is supported in part by grants from NSF and DOE. Lamont-Doherty contribution no. 5029.

References cited

Ball, M.C., and Taylor, H.F.W. (1961) The dehydration of brucite. Mineralogical Magazine, 32, 754–766.

Barnes, H.L., and Ernst, W.G. (1963) Ideality and ionization in hydrothermal fluids: The system MgO-H_2O-NaOH. American Journal of Science, 261, 129–150.

Belonoshko, A., and Saxena, S.K. (1991) A molecular dynamics study of the pressure-volume-temperature properties of super-critical fluids. I. H_2O Geochimica et Cosmochimica Acta, 55, 381–387.

Bowen, N.L., and Tuttle, O.F. (1949) The system MgO-SiO_2-H_2O. Geological Society of America Bulletin, 60, 439–460.

Brodholt, J., and Wood, B. (1990) Molecular dynamics of water at high temperatures and pressures. Geochimica et Cosmochimica Acta, 54, 2611–2616.

Buchwald, V.F., Kjer, T., and Thorsen, K.A. (1985) Thermal migration. I. Or how to transport iron sulfide in solid iron meteorites. Meteoritics, 20, 617–618.

Burnham, C.W., Holloway, J.R., and Davis, N.F. (1969) Thermodynamic properties of water to 1000 °C and 10,000 bars. Geological Society of America Special Paper, 132, 96 p.

Carnahan, N.F., and Starling, K.E. (1972) Intermolecular repulsions and the equation of state for fluids. American Institute of Chemical Engineering, 18, 1184–1189.

Duffy, T.S., Ahrens, T.J., and Lange, M.A. (1991) The shock wave equation of state of brucite $Mg(OH)_2$. Journal of Geophysical Research, 96, 14319–14330.

Ellis, D.E., and Wyllie, P.J. (1979) Carbonation, hydration, and melting relations in the system MgO-H_2O-CO_2 at pressures up to 100 kbar. American Mineralogist, 64, 32–40.

Gasparik, T., and Zhang, J. (1992) Stability of hydrous phases at pressures corresponding to the Earth's transition zone. Eos, 73, 53.

Getting, I.C., and Kennedy, G.C. (1970) Effect of pressure on the emf of chromel-alumel and platinum-platinum 10% rhodium thermocouples. Journal of Applied Physics, 41, 4552–4562.

Halbach, H., and Chatterjee, N.D. (1982) An empirical Redlich-Kwong-type equation of state for water to 1000 °C and 200 kbar. Contributions to Mineralogy and Petrology, 79, 337–345.

Holland, T.J.B., and Powell, R. (1990) An enlarged and updated internally consistent thermodynamic dataset with uncertainties and correlations: The system K_2O-Na_2O-CaO-MgO-MnO-FeO-Fe_2O_3-Al_2O_3-TiO_2-SiO_2-C-H_2-O_2. Journal of Metamorphic Geology, 8, 89–124.

Holloway, J.R. (1981) Volatile interactions in magmas. In R.C. Newton, A. Navrotsky, and B.J. Wood, Eds., Thermodynamics of minerals and melts, p. 273–293. Springer-Verlag, New York.

Irving, A.J., Huang, W.L., and Wyllie, P.J. (1977) Phase relations of portlandite, $Ca(OH)_2$, and brucite, $Mg(OH)_2$, to 33 kilobars. American Journal of Science, 277, 313–321.

Jackson, I., and Niesler, H. (1982) The elasticity of periclase to 3 GPa and some geophysical implications. In S. Akimoto and M. H. Manghnani, Eds., High pressure research in geophysics, p. 93–133. Center for Academic Publishing, Tokyo.

Johnson, M.C., Walker, D., and Saxena, S. (1991) Brucite dehydration and the compressibility of water at very high pressures. Eos, 72, 564.

Kanzaki, M. (1990) Thermal analysis in a multi-anvil high-*P* apparatus. Eos, 71, 1697.

——— (1991) Dehydration of brucite ($Mg(OH)_2$) at high pressure detected by differential thermal analysis. Geophysical Research Letters, 18, 2189–2192.

Kerrick, D.M., and Jacobs, G.K. (1981) A modified Redlich-Kwong equation for H_2O, CO_2, and H_2O-CO_2 mixtures at elevated pressures and temperatures. American Journal of Science, 281, 735–767.

King, E.G., Ferrante, M.J., and Pankratz, L.B. (1975) Thermodynamic data for $Mg(OH)_2$ (brucite). United States Bureau of Mines Report of Investigations, 8041, 13 p.

Leinenweber, K., Weidner, D.J., Vaughan, M., Shimomura, O., Kato, T., Morijima, H., Chen, J., and Kikegawa, T. (1991) In-situ x-ray study of the dehydration of brucite. Eos, 72, 437.

Lesher, C.E., and Walker, D. (1988) Cumulate maturation and melt migration in a temperature gradient. Journal of Geophysical Research, 93, 10295–10311.

Lyzenga, G.A., Ahrens, T.J., Nellis, W.J., and Mitchell, A.C. (1982) The temperature of shock-compressed water. Journal of Chemistry and Physics, 76, 6282–6286.

Meade, C., and Jeanloz, R. (1991) Deep-focus earthquakes and recycling of water into the Earth's mantle. Science, 252, 68–72.

Ohtani, E. (1979) Melting relation of Fe_2SiO_4 up to about 200 kbar. Journal of the Physics of the Earth, 27, 189–208.

Redlich, O., and Kwong, J.N.S. (1949) On the thermodynamics of solutions. V. An equation of state. Chemical Reviews, 44, 233–244.

Rice, M.H., and Walsh, J.M. (1957) Equation of state of water to 250 kilobars. The Journal of Chemical Physics, 26, 824–830.

Robie, R.A., Hemingway, B.S., and Fisher, J.R. (1979) Thermodynamic properties of minerals and related substances at 298.15 K and 1 bar pressure and at higher temperatures. Geological Survey Bulletin, 1452, 456 p.

Roy, D.M., and Roy, R. (1957) A redetermination of equilibria in the system MgO-H_2O and comments on earlier work. American Journal of Science, 255, 573–582.

Saxena, S.K. (1989) Assessment of bulk modulus, thermal expansion and heat capacity of minerals. Geochemica Cosmochemica Acta, 53, 785–789.

Saxena, S.K., and Zhang, J. (1989) Assessed high-temperature thermochemical data on some solids. Journal of Physics and Chemistry of Solids, 50, 723–727.

Schramke, J.A., Kerrick, D.M., and Blencoe, J.G. (1982) Experimental determination of the brucite = periclase + water equilibrium with a new volumetric technique. American Mineralogist, 67, 269–276.

Walker, D. (1991) Lubrication, gasketing, and precision in multianvil experiments. American Mineralogist, 76, 1092–1100.

Walker, D., Jurewicz, S.R., and Watson, E.B. (1988) Adcumulus dunite growth in a small thermal gradient. Contributions to Mineralogy and Petrology, 99, 306–319.

Walker, D., Carpenter, M.A., and Hitch, C.M. (1990) Some simplifications to multianvil devices for high pressure experiments. American Mineralogist, 75, 1020–1028.

Weber, J.N., and Roy, R. (1965) Complex stable ↔ metastable solid reactions illustrated with the $Mg(OH)_2$ ↔ MgO reaction. American Journal of Science, 263, 668–677.

Williams, D.W., and Kennedy, G.C. (1969) Melting curve of diopside to 50 kilobars. Journal of Geophysical Research, 74, 4359–4366.

Yamaoka, S., Fukunaga, O., and Saito, S. (1970) Phase equilibria in the system MgO-H_2O at high temperatures and very high pressures. Journal of the American Ceramic Society, 53, 179–181.

Manuscript received April 16, 1992
Manuscript accepted November 25, 1992